Soft Matter

RSC Publishing

PAPER

View Article Online
View Journal | View Issue

Cite this: *Soft Matter*, 2013, **9**, 4437

Kinetics of colloidal gelation and scaling of the gelation point

Hua Wu,*[a] Jian-jun Xie[b] and Massimo Morbidelli*[a]

Received 11th January 2013
Accepted 25th February 2013

DOI: 10.1039/c3sm00117b

www.rsc.org/softmatter

We have investigated *in situ* the colloidal gelation in the RLCA regime using a small-angle light scattering technique, avoiding any sample handling, in the particle volume fraction range of 0.02 to 0.08, and observed some specific gelation features never indicated previously. The measured structure evolutions clearly show that colloidal gelation follows two stages: (1) cluster growth and (2) cluster interconnection when crowded to form the gel. In Stage 1, the aggregation kinetics in all the cases follows the power-law scaling, as if it is in the DLCA regime. This indicates that crossover from RLCA to DLCA kinetics takes place along the gelation process. When an appropriate dimensionless time is defined to account for the role of particle concentration and stability, all the kinetic data in Stage 1 obtained at different particle sizes and concentrations and different salt concentrations collapse to form a single master curve. Thus, all the gelation systems follow the same aggregation kinetics and the formed clusters have the same structure. In Stage 2, the average clusters grow only slightly with time. This allows us to distinctly determine the gelation point by the transition from the aggregation kinetics before the gelation point to the slow cluster growth in the gel. It is found that at the gelation point, the volume fraction occupied by all the clusters is constant, independent of the particle volume fraction. This is strong evidence that for a given colloid, the same crowding condition has to be reached in order to start the percolation forming a gel. Interestingly, this crowding condition depends on the particle size. It is observed that the occupied volume fraction at the gelation point is substantially larger for a colloid with a smaller particle radius than for a colloid with a larger radius.

1 Introduction

Liquid-like colloidal dispersions may dynamically arrest or jam to form solid-like materials, whose properties can be substantially different from their original disperse states, leading to wide applications in many areas such as in producing ceramics, food, medicine, controlled porous materials, and drug delivery devices, *etc.* Thus, in recent years, dynamic arrest of colloidal systems has received great scientific attention.[1–22]

One of the most widely studied liquid-like to solid-like transitions is related to the mass fractal growth of clusters during the so-called diffusion-limited cluster aggregation (DLCA)[4–8] or reaction-limited cluster aggregation (RLCA).[9–12] The bonding among the particles in these cases is typically located at the deep well of the interaction potential, and thus in most cases it is irreversible. The liquid-like to solid-like transition is believed to result from interconnections of the mass fractal clusters when they grow and fill the entire available space. The formed solid-like matter is called a gel, and the process is generally referred to as colloidal gelation.

The most suitable techniques for monitoring the growth of the fractal clusters in a colloidal system are scatterings, particularly light scattering, because the size of the clusters can reach several microns. However, in the case of colloidal gelation to realize a standing solid-like gel, the particle volume fraction ϕ has to be significantly large (*e.g.*, $\phi \geq 0.02$).[8] In this case, the gelation system is rather turbid for most colloidal systems. Thus, typically one cannot monitor *in situ* with light scattering instruments the growth of clusters with time and their interconnection to form a gel. In fact, to investigate the gelation kinetics, one often has to take samples from the gelation system, dilute and quench them, and then characterize them by light scattering.[23] However, this procedure is feasible only when the clusters are small and the aggregation process is far from the gelation point. Close to the gelation point, the clusters start to interconnect, and it is difficult to take a sample that can correctly represent the system. Particularly after the gelation point, it becomes impossible to take a sample without altering the gel structure. Thus, detailed investigations of the aggregation behavior around the gelation point and the structure of the final gels using light scattering techniques for $\phi \geq 0.02$ have seldomly been reported in the literature.

[a]*Institute for Chemical and Bioengineering, Department of Chemistry and Applied Bioscience, ETH Zurich, 8093 Zurich, Switzerland. E-mail: hua.wu@chem.ethz.ch; massimo.morbidelli@chem.ethz.ch*

[b]*Institute of Materials Science and Engineering, Central South University of Forestry and Technology, Changsha 410004, Hunan, China*

In our previous work,[12,24] we were able to *in situ* characterize the entire scattering structure factors of colloidal gels formed in the RLCA regime at particle volume fractions in the range of $0.02 \leq \phi \leq 0.08$, covering a wavevector range of 5 orders of magnitude by combining small-angle and wide-angle light scattering, and small-angle neutron scattering techniques. We succeeded in performing such scattering measurements of the gels, owing to the applied fluorinated polymer colloids (Hyflon® MFA latexes), which have a very low optical contrast with respect to water. In fact, the formed gels were transparent. It is worth noting that the combination of such transparent gels and three scattering devices mentioned above generates unique scattering data in the literature, thus providing unique information on the gel structure. It is particularly worth mentioning the portion of the scattering structure factor characterized by small-angle light scattering (SALS), which covers not only the structure level of the clusters constituting the gel but also the gel structure above the cluster level. The latter is found to exhibit a surface fractal scaling.

In the present study, we work further with the above fluorinated polymer colloids (Hyflon® MFA latexes) under concentrated conditions. We mainly focus on *in situ* investigation of, instead of the gel structure, the gelation kinetics both before and after the gelation point. We would like to understand how the liquid-like to solid-like transition occurs from the light scattering information, and how the colloidal particle size and the gelation conditions affect the transition, hopefully to gain further insight into the mechanism of colloidal gelation. To this aim, the SALS technique is the most suitable one, because it covers the structure levels of both the clusters and the gels.

2 The gelation experiments

2.1 The colloidal gelation systems

Two fluorinated polymer MFA colloids, charge ($-COO^-$) stabilized and supplied by Solvay Italy, are used to perform the gelation experiments. The only difference between the two colloids is the radius of the primary particles, $R_p = 21$ nm and 37.5 nm, respectively, which is determined by fitting the form factors measured experimentally with the RDG (Rayleigh–Debye–Gans) expression for spheres.[25] The original particle volume fractions were 0.0642 and 0.149, for the colloids with $R_p = 21$ nm and 37.5 nm, respectively. Since the colloid needs to mix with a salt solution to initiate the gelation, the range of the particle volume fraction for gelation is limited ($\phi \in [0.02, 0.05]$) for the colloid with $R_p = 21$ nm, while for the colloid with $R_p =$ 37.5 nm, the ϕ range can be larger ($\phi \in [0.02, 0.08]$). Note that for $\phi < 0.02$, the formed gel is too weak to fill the full space, because at a certain point the gel collapses leading to phase separation. For $\phi > 0.08$, the system becomes significantly turbid as the gelation process proceeds, and the multiple scattering may affect the characterization results.

All the gelation experiments were performed in the RLCA regime, and NaCl was used to destabilize the colloids. The gelation was initiated by pouring together latex and NaCl solution of roughly the same volume into a bottle, followed by gentle shaking. The obtained mixture was then immediately introduced into the measurement cells of the scattering instruments. More details about the procedure for initiating the gelation process can be found elsewhere.[25] Conditions for all the gelation systems investigated here are listed in Table 1.

2.2 The gelation kinetic data from the scattering structure factor

A small-angle light scattering (SALS) instrument, Mastersizer 2000 (Malvern, UK) with a He–Ne laser (wavelength = 632 nm) and a flat cell (thickness = 2.4 mm), was used to monitor the gelation kinetics. All of the gelation processes were performed directly in the SALS cell, so as to avoid sampling-induced errors. Since the SALS instrument requires only 10–20 seconds to obtain an intensity curve with good statistics, this time is negligible with respect to the time required for the gelation. Thus, the time evolution of the measured intensity curve represents true structure evolution of the clusters and gel along the gelation process.

Fig. 1 shows an example of the time evolution of the scattering structure factor obtained from the SALS instrument, as the ratio of the intensity curves $I(q)$ to the experimental form factor $P(q)$, corresponding to Gelation System 5 in Table 1. As already discussed in our previous works,[12,24] the structure factor curves in Fig. 1 can be divided into two regions: the first region corresponds to $q > 1 \times 10^{-3}$ nm^{-1}, which represents the growth of the mass fractal clusters as the gelation process proceeds. The second region corresponds to $q < 1 \times 10^{-3}$ nm^{-1}, which reveals the evolution of the surface fractal scaling, thus being present only after reaching the gelation point. Note that the final gel was characterized by combining SALS, WALS (wide-angle light scattering) and SANS (small-angle neutron scattering) instruments, and the scattering structure factor at $t =$ 2163 min in Fig. 1 represents the obtained result. In particular, the slope of the power-law regime in $q > 1 \times 10^{-3}$ nm^{-1} gives the apparent mass fractal dimension ($\langle D_m \rangle$) of the clusters constituting the gel, while the power-law regime in $q < 1 \times 10^{-3}$ nm^{-1}, with the absolute value of the slope greater than 3, reflects the surface fractal scaling. Detailed analysis of the entire structure factor was presented in our previous reports.[12,24]

Table 1 Values of the parameters for all the gelation systems investigated in this work

Gelation system	ϕ	R_p nm	C_s mM	W
1	0.02	21	66.0	3.35×10^5
2	0.03	21	63.0	5.25×10^5
3	0.04	21	50.0	2.52×10^7
4	0.04	21	55.0	3.70×10^6
5	0.04	21	60.0	1.05×10^6
6	0.05	21	58.0	1.39×10^6
7	0.02	37.5	22.4	2.68×10^5
8	0.04	37.5	20.0	7.45×10^5
9	0.06	37.5	18.0	1.65×10^6
10	0.06	37.5	18.5	8.50×10^5
11	0.08	37.5	15.5	1.32×10^7
12	0.08	37.5	16.0	6.75×10^6

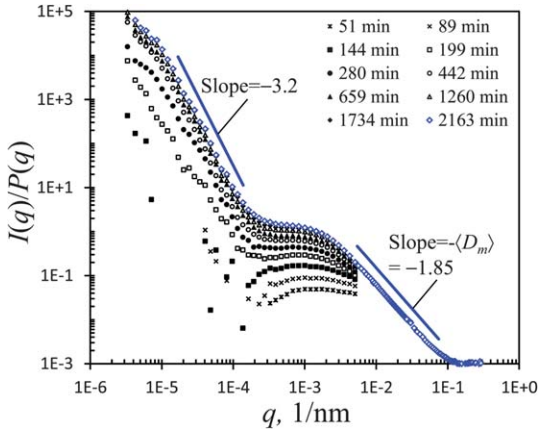

Fig. 1 Time evolution of the scattering structure factor, $I(q)/P(q)$, measured by the SALS instrument for the particles with $R_p = 21$ nm at $\phi = 0.04$ and $C_s = 60$ mM. The legend shows the time elapsed after initiating the aggregation. The final scattering structure factor at $t = 2163$ min was obtained by combining SALS, WALS and SANS.

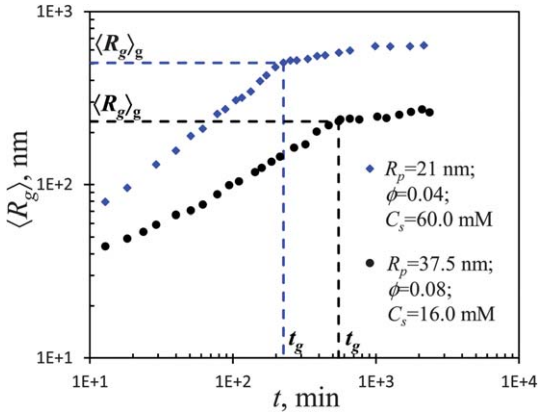

Fig. 2 Examples of the time evolutions of the average radius of gyration $\langle R_g \rangle$ for the colloids with $R_p = 21$ nm and 37.5 nm, respectively. The location where the transition from a faster to a slower $\langle R_g \rangle$ growth rate occurs is defined here as the gelation point.

It should be pointed out that the structure factor in Fig. 1 clearly shows that the colloidal gelation process results from two stages: (1) growth of clusters, leading to system crowding, and (2) interconnection of clusters to form the gel. The gel structure above the cluster level is completely different from that of the clusters. Thus, the focus of this work is within the level of the clusters constituting the gel. We investigate the kinetics of the cluster growth both before and after reaching the gelation point. To this aim, we have treated all the scattering structure factors in the cluster growth region, based on the Guinier plot, to obtain the time evolution of the average radius of gyration of the clusters, $\langle R_g \rangle$, thus representing the gelation kinetics.

3 Results and discussion

3.1 The gelation kinetics

In the case of $R_p = 37.5$ nm, the gelation kinetics was previously investigated using a WALS instrument.[26,27] Due to the long characterization time of the WALS technique with a goniometer system, the gelation kinetics was monitored through a sampling-dilution procedure. This procedure is feasible only when the clusters are small and the aggregation process is far from the gelation point. Close to the gelation point, clusters start to interconnect, and it is difficult to take a sample that can correctly represent the system. Particularly after the gelation point, it becomes impossible to take a sample without altering the gel structure. When the SALS instrument is applied in the present work, the very short characterization time enables us to *in situ* monitor the aggregation kinetics and cluster structure along the entire gelation process, without sampling and disturbing the process.

Fig. 2 reports the typical time evolutions of the average radius of gyration $\langle R_g \rangle$ along the gelation process for the colloids with $R_p = 21$ nm and 37.5 nm, respectively. Both the $\langle R_g \rangle$ curves have a common feature that there is a clear transition from a faster growth rate to a much slower growth rate. For example, in the case of $R_p = 21$ nm, $\phi = 0.04$ and $C_s = 60$ mM in Fig. 2, such a transition occurs at $t = 226$ min, as indicated by the broken line. From the corresponding time evolution of the scattering structure factor in Fig. 1, at the given time a well-defined surface fractal scaling appears, thus representing the transition from aggregation to gelation. In fact, after reaching this time, the system ceases to flow as revealed by visual observation. Therefore, along the gelation kinetics, the time at which the transition from a faster to a slower $\langle R_g \rangle$ growth rate occurs is defined here as the gelation time, t_g, and the corresponding $\langle R_g \rangle$ is referred to as the critical $\langle R_g \rangle$ for gelation, $\langle R_g \rangle_g$. It follows that the region with $t < t_g$ corresponds to the kinetics of cluster growth, till reaching the gelation point, while for the region with $t > t_g$, the small increase in $\langle R_g \rangle$ should be related to the progressive attachment of the remaining small free clusters to the gel network.

In Fig. 3 we have shown the time evolution of the measured $\langle R_g \rangle$ for all the gelation systems listed in Table 1. Note that for each case in the legend there are two values: the first is the particle volume fraction ϕ and the second is the salt concentration C_s in mM. It is seen that the $\langle R_g \rangle$ curves in Fig. 3 are rather arbitrarily located. This arises because different NaCl and particle concentrations are used for different gelation systems, leading to different colloidal stability and aggregation rates. To account for the effect of salt and particle concentrations on the kinetics, let us plot all the $\langle R_g \rangle$ data in Fig. 3 as a function of the dimensionless aggregation time τ, defined as follows:[28]

$$\tau = \frac{K_B N_0 t}{W} \quad (1)$$

where K_B ($=8kT/3\mu$, with k the Boltzmann constant, T temperature and μ kinematic viscosity) is the Smoluchowski aggregation rate constant, N_0 the initial number concentration of the primary particles, and W the Fuchs stability ratio. The W value in eqn (1) has been estimated from the initial stage of the aggregation kinetics,[28,29] and reported in Table 1 for each system. In Fig. 4a and b are shown the $\langle R_g \rangle / R_p$ *vs.* τ curves,

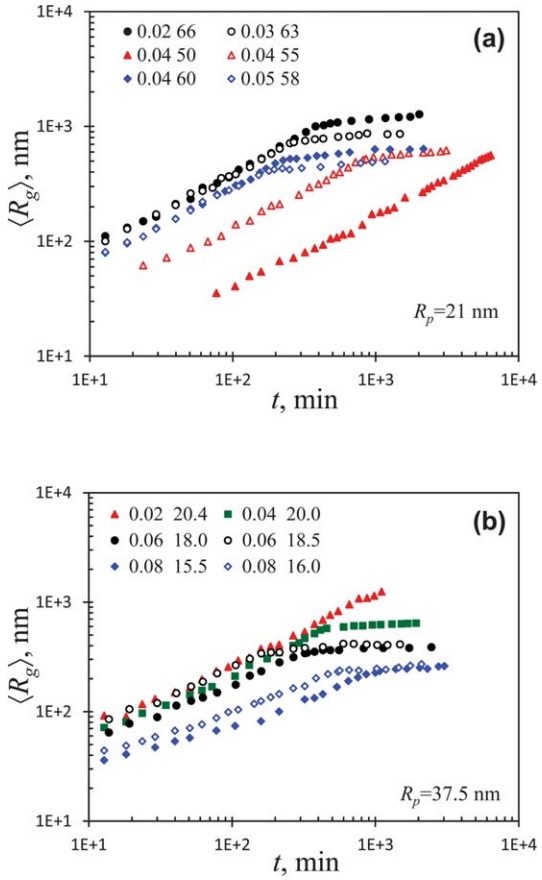

Fig. 3 Time evolutions of the average radius of gyration, $\langle R_g \rangle$, for all the gelation systems listed in Table 1, using colloids with (a) $R_p = 21$ nm and (b) $R_p = 37.5$ nm. The first and second values in the legend are the particle volume fraction ϕ and the salt concentration C_s in mM, respectively.

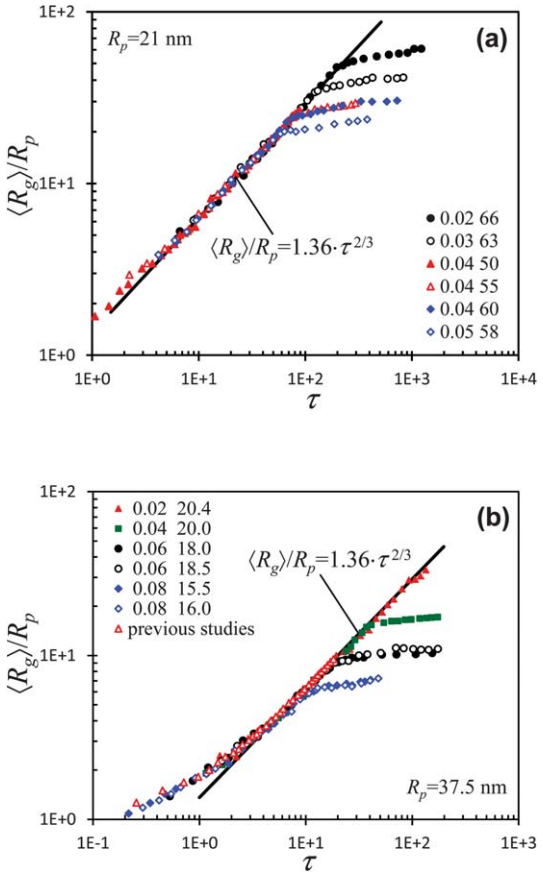

Fig. 4 The $\langle R_g \rangle$ data in Fig. 3 plotted in the form of $\langle R_g \rangle / R_p$ *vs.* the dimensionless time, τ, defined by eqn (1). The open triangles in (b) are experimental data obtained in previous work.[27]

corresponding to the $\langle R_g \rangle$ data in Fig. 3a and b, respectively. It is seen that in this way, all the $\langle R_g \rangle / R_p$ data for $\tau < \tau_g$ obtained at different C_s and ϕ values collapse to form a single master curve. Moreover, if all the $\langle R_g \rangle / R_p$ data for $\tau < \tau_g$ in Fig. 4a and b for $R_p = 21$ nm and 37.5 nm, respectively, are plotted together, they also collapse to a single master curve. Considering that the dimensionless time τ has accounted for the effect of the colloidal stability (W) and particle concentration (N_0) on the aggregation rate, this result indicates that for $\tau < \tau_g$ all the gelation systems in Table 1 follow the same aggregation kinetics and the formed clusters have the same structure, independent of the salt concentration, particle volume fraction and primary particle size.

In a previous work,[27] a similar study on the aggregation kinetics was carried out using the same colloid with $R_p = 37.5$ nm, but through an off-line sampling-dilution procedure, and the average cluster sizes were characterized using a WALS instrument. In that work, a $\langle R_g \rangle / R_p$–$\tau$ master curve for the kinetics before reaching the gelation point was also obtained, which has been reproduced here in Fig. 4b (open triangles). It is seen that the agreement between the previous and the present master curves is excellent. This confirms the reliability of the kinetic data measured through both *in situ* SALS and off-line WALS experiments.

It is well known that in the RLCA regime, the average cluster size grows exponentially with time. The results in Fig. 4 however show that after an initial stage of the aggregation process, the kinetic data in both cases of $R_p = 21$ nm and 37.5 nm follow a power-law scaling (as represented by the straight line), similar to that of a DLCA process. This clearly indicates that in all the cases crossover from the RLCA to DLCA regime occurs.[30] In principle, the exponent of the power-law scaling for the DLCA process must be equal to the reciprocal of the mass fractal dimension, $1/D_m = 1/1.8 \approx 0.55$, while in Fig. 4 it is $2/3 = 0.67$, significantly larger. This may arise from the crowding effect of the clusters in this stage. As observed from both Monte-Carlo simulations[31] and experiments[32] near the gelation point, the growth of the clusters accelerates.

Another important observation from Fig. 4 is that for those sets of experiments carried out at different salt concentrations but at the same particle volume fraction, the $\langle R_g \rangle / R_p$ data collapse not only in the region of $\tau < \tau_g$, but also in the region of $\tau > \tau_g$. This may indicate that although the small free clusters caged inside the gel network do not follow the same kinetics as that induced by the random Brownian motion and most probably just attach to the local gel network, such an "attachment" process is rather similar, independent of the salt concentration. This gives rise to the consequence that for a given colloid at the

same particle volume fraction, the dimensionless gelation time is independent of the salt concentration, and so is the average cluster size at the gelation point, $\langle R_g \rangle_g$.

3.2 Scaling of the average cluster size at the gelation point

After reaching the gelation point (*i.e.*, $\tau > \tau_g$), the fact that the $\langle R_g \rangle / R_p$ data do not collapse to a single master curve evidences that the gelation time and the corresponding average cluster size, τ_g and $\langle R_g \rangle_g$, are functions of the particle volume fraction, ϕ. We have collected the $\langle R_g \rangle_g$ values from both colloids with $R_p = 21$ nm and 37.5 nm in Fig. 4 and plotted them in Fig. 5a as a function of ϕ. It is interesting to have found that the two sets of the $\langle R_g \rangle_g$ values from different primary particle radii collapse to a single curve. This indicates that at the same particle volume fraction, the average cluster size at the gelation point, $\langle R_g \rangle_g$, is the same for the two colloids with $R_p = 21$ nm and 37.5 nm, respectively. To better understand the consequence of the observed behavior, let us estimate the volume fraction occupied by all the clusters at the gelation point, ϕ_g, based on $\langle R_g \rangle_g$, which can be simply expressed as

$$\phi_g = \frac{N_0}{\langle i \rangle_g} \frac{4}{3} \pi \langle R_g \rangle_g^3 \quad (2)$$

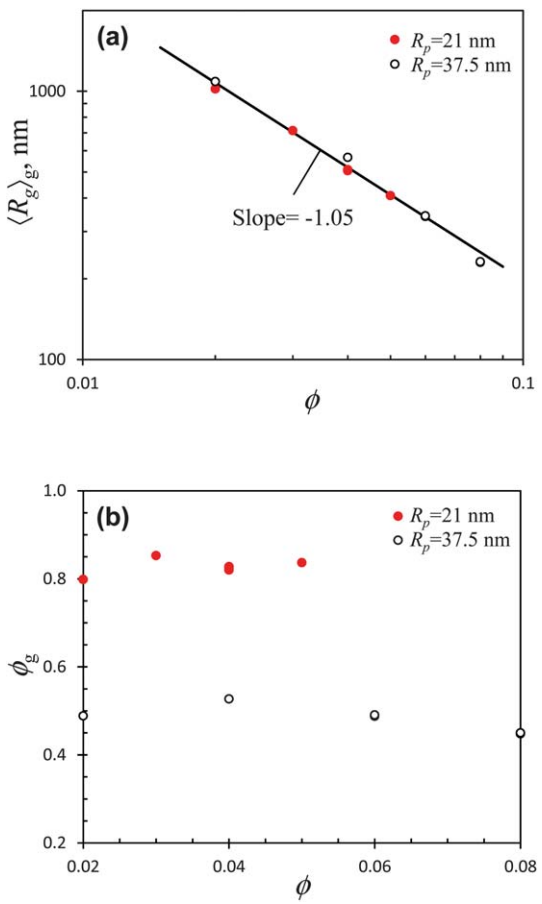

Fig. 5 The average radius of gyration $\langle R_g \rangle_g$ at the gelation point (a) and the corresponding volume fraction occupied by all the clusters in the system (b), as a function of ϕ, in both cases of $R_p = 21$ nm and $R_p = 37.5$ nm.

with $\langle i \rangle_g$ the mass of an average cluster at the gelation point, which follows the fractal scaling,

$$\langle i \rangle_g = k \left(\frac{\langle R_g \rangle_g}{R_p} \right)^{D_m} \quad (3)$$

where the prefactor k is found from intense numerical simulations to be a function of the mass fractal dimension D_m:[33]

$$k = 4.46 D_m^{-2.08} \quad (4)$$

Substituting eqn (3) and (4) into (2), after suitable arrangement, we have

$$\phi_g = \frac{\phi}{4.46 D_m^{-2.08}} \left(\frac{\langle R_g \rangle_g}{R_p} \right)^{3-D_m} \quad (5)$$

Assuming $D_m = 2.05$, typical of RLCA clusters, we have computed the ϕ_g values using the $\langle R_g \rangle_g$ values in Fig. 5a, and the results are shown in Fig. 5b. It is seen that for a given colloid with $R_p = 21$ nm or $R_p = 37.5$ nm, the estimated ϕ_g value is practically constant, independent of ϕ. This clearly demonstrates that interconnection of clusters to form a gel network is under the same crowding conditions, or in other words, even though for a larger particle volume fraction the critical average cluster size, $\langle R_g \rangle_g$, is smaller, the volume fraction occupied by all the clusters has to reach the same level in order to start the percolation forming the gel network. Further, since now ϕ_g is constant at the gelation point, it can be easily derived from eqn (5) that $\langle R_g \rangle_g \propto \phi^{-1/(3-D_m)}$. Then, with $D_m = 2.05$ for RLCA clusters, we have $\langle R_g \rangle_g \propto \phi^{-1.05}$, *i.e.*, in the log–log plane, the slope of the scaling between $\langle R_g \rangle_g$ and ϕ must be equal to -1.05. This is in excellent agreement with the result in Fig. 5a.

On the other hand, it is interesting to have found that the occupied volume fraction by the clusters at the gelation point is substantially larger for $R_p = 21$ nm ($\phi_g \sim 0.8$) than for $R_p = 37.5$ nm ($\phi_g \sim 0.5$). This may be related to the fact that in Fig. 5a at the same ϕ value, the $\langle R_g \rangle_g$ value is the same for $R_p = 21$ nm and 37.5 nm, and it follows that $\langle R_g \rangle_g / R_p$ is larger for $R_p = 21$ nm than for $R_p = 37.5$ nm. Then, for $R_p = 21$ nm, the particle density in the external region of the cluster is much lower such that the clusters can (and have to) interpenetrate into each other to a larger extent in order to form a standing solid network. In this way, the required volume fraction of the clusters is certainly larger for $R_p = 21$ nm.

It should be mentioned that since the density of the applied polymer particles is 2.14 kg L^{-1}, more than twice as high as that of water, it is necessary to examine if cluster sedimentation may affect the aggregation/gelation process. In a previous work,[28] we have estimated in the case of MFA the critical cluster size (R_{crit}/R_p) as a function of ϕ, at which the sedimentation and the diffusion characteristic times become identical. When $(R_g/R_p) > (R_{crit}/R_p)$, the sedimentation characteristic time becomes smaller than the diffusion one, and the cluster sedimentation plays a dominant role. It was found that the estimated R_{crit}/R_p value increases as ϕ increases, and $R_{crit}/R_p > 55$ for $\phi \geq 0.02$. When we applied this result to our data in Fig. 4, it is seen that

all the $\langle R_g \rangle / R_p$ values before the gelation point are smaller than 55. Thus, the cluster sedimentation does not play a significant role in all our gelation systems.

3.3 Scaling of the gelation time

The values of the dimensionless gelation time, τ_g, obtained from Fig. 4 are reported in Fig. 6a as a function of ϕ. As expected, the dimensionless gelation time decreases as the particle volume fraction increases, in a power-law scaling. However, unlike the average cluster size, $\langle R_g \rangle_g$ in Fig. 5a, the τ_g values obtained from the colloids with $R_p = 21$ nm and 37.5 nm do not collapse to a single curve. More surprisingly, at a given particle volume fraction, the τ_g value is larger for $R_p = 21$ nm than for $R_p = 37.5$ nm. When one considers that at a fixed ϕ value in Fig. 5a the $\langle R_g \rangle_g$ value is the same for $R_p = 21$ nm and 37.5 nm, the results in Fig. 6a indicate that at a fixed ϕ value the time for reaching the defined cluster size, $\langle R_g \rangle_g$, is longer for $R_p = 21$ nm than for $R_p = 37.5$ nm. We believe that this is a consequence of the required crowding extent at the gelation point that is larger for $R_p = 21$ nm ($\phi_g \sim 0.8$) than for $R_p = 37.5$ nm ($\phi_g \sim 0.5$), as shown in Fig. 5b. In fact, if we assume that the ϕ_g value for $R_p = 21$ nm is the same as for $R_p = 37.5$ nm, *i.e.*, $\phi_g = 0.5$, we can first compute from eqn (5) the $\langle R_g \rangle_g$ values (which are naturally smaller than those in Fig. 5a), and then estimate the τ_g values from the scaling in Fig. 4. The τ_g values obtained in this way for $R_p = 21$ nm are shown in Fig. 6b, together with the experimentally measured τ_g values for $R_p = 37.5$ nm. It is seen that now the τ_g values from both $R_p = 21$ nm and 37.5 nm collapse to a single curve. It is therefore confirmed that the difference in the gelation time between $R_p = 21$ nm and 37.5 nm in Fig. 6a is related to different requirements in the system crowding at the gelation point.

The power-law scaling of τ_g *vs.* ϕ in Fig. 6 has an exponent of -1.6. To derive such a value, we need to go back to the aggregation kinetic behaviour in Fig. 4, where we have observed the following scaling before the gelation point:

$$\frac{\langle R_g \rangle}{R_p} = 1.36\tau^{2/3}, \tag{6}$$

which the gelation point [τ_g, $\langle R_g \rangle_g$] should satisfy as well. From eqn (5), considering that ϕ_g is constant, we have $\langle R_g \rangle_g / R_p \propto \phi^{-1/(3-D_m)}$, which when substituted into eqn (6) at the gelation point leads to

$$\tau_g \propto \phi^{-\frac{3}{2(3-D_m)}} \tag{7}$$

With $D_m = 2.05$ for RLCA clusters, we have the exponent in eqn (7) equal to -1.6, equal to that in Fig. 6. Thus, the scaling behavior in Fig. 6 is a consequence of the kinetic behavior in Fig. 4.

In Fig. 6a, we have also reported two τ_g values for the colloid with $R_p = 37.5$ nm determined previously based on elastic modulus, through small amplitude oscillatory shearing experiments.[27] The two values are significantly larger than those obtained in the present work through *in situ* SALS experiments. This may reveal that even though the shearing force is very small (strain = 0.1% and frequency = 10 rad s^{-1}), it is still possible to disturb and delay the interconnection among the clusters. Moreover, since the two points merge into the scaling of the colloid with $R_p = 21$ nm in Fig. 6a, it indicates that the occupied volume fraction by the clusters at the gelation point becomes $\phi_g \sim 0.8$ in the oscillatory shearing experiment.

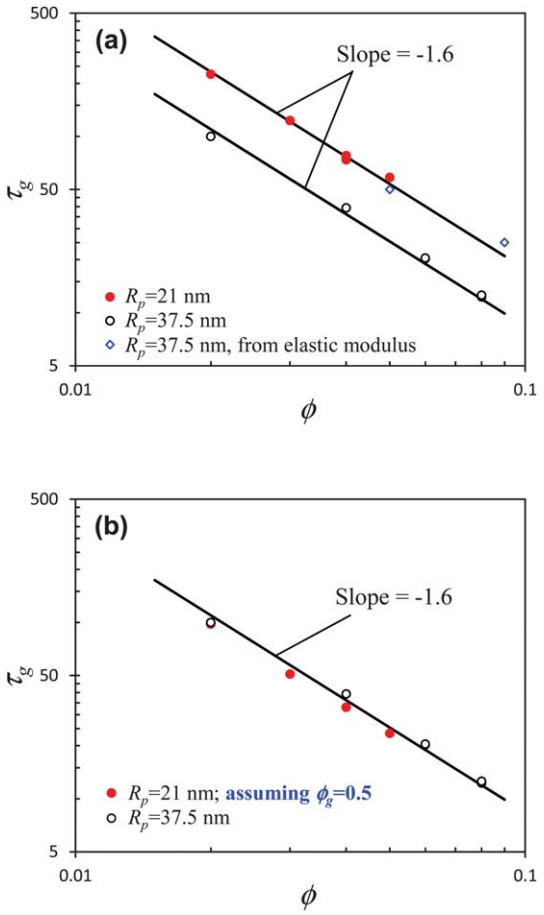

Fig. 6 (a) The dimensionless gelation time τ_g as a function of ϕ obtained from Fig. 4 in both cases of $R_p = 21$ nm and $R_p = 37.5$ nm and (b) the τ_g values for $R_p = 21$ nm have been estimated by assuming $\phi_g = 0.5$, instead of $\phi_g \sim 0.8$ as given in Fig. 5b. The open diamonds in (a) represent experimental data obtained in previous work.[27]

4 Concluding remarks

In this work, the colloidal gelation kinetics in the RLCA regime, in the range of particle volume fractions, $0.02 \leq \phi \leq 0.08$, have been investigated *in situ* using a small-angle light scattering (SALS) technique, avoiding any handling for sampling and characterization. To this aim, at such high particle concentrations, we have performed the gelation using fluorinated polymer colloids, Hyflon MFA® latexes, with particle radius, $R_p = 21$ nm and 37.5 nm, respectively. These particles have a very low optical contrast with respect to water, thus allowing us to monitor the cluster evolution in the SALS cell till forming a gel and to discover some specific features about gelation that have never been observed before.

From the time evolution of the measured structure factor, it is clearly evidenced that the colloidal gelation follows two

stages: (1) growth of clusters with time and (2) interconnection of clusters due to crowding to form the gel. In Stage 1, after an initial interval of cluster growth, the aggregation kinetics in all the cases follows the power-law scaling, as if it is in the DLCA regime. This clearly indicates that crossover from RLCA to DLCA kinetics takes place along the gelation process. Moreover, all the $\langle R_g \rangle$ values in Stage 1 obtained at different particle volume fractions, salt concentrations and particle radii collapse to a single master curve when they are plotted in the form of $\langle R_g \rangle / R_p$ *vs.* the dimensionless time, τ, defined by eqn (1), which accounts for the effect of the colloidal stability and particle concentration. This result indicates that all the gelation systems follow the same aggregation kinetics and the formed clusters have the same structure, independent of the salt concentration, particle volume fraction and primary particle size.

In Stage 2, the identity of the average clusters constituting the gel can be always observed within the gel, and their size still grows slightly with time, due to attachment of the remaining small free clusters to the gel network. Owing to the slower growth rate of the clusters after gelation, with respect to that in Stage 1, the gelation point for each system has been distinctly defined from the time evolution of $\langle R_g \rangle$. In addition, for those gelation systems with the same particle volume fraction and primary particle size, the $\langle R_g \rangle / R_p$ *vs.* τ curves collapse not only in Stage 1 but also in Stage 2. It follows that in this dimensionless plane, for a given colloid the gelation point is uniquely defined by the particle volume fraction, independent of the salt concentration.

At the gelation point, the radius of gyration of the clusters, $\langle R_g \rangle_g$, decreases as the particle volume fraction increases, while the volume fraction occupied by all the clusters, ϕ_g, estimated using $\langle R_g \rangle_g$, is constant, independent of the particle volume fraction. This is strong evidence that for a given colloid, the same crowding condition has to be reached in order to start the percolation forming a gel. On the other hand, it is interesting to have found for the first time that the ϕ_g value at the gelation point depends substantially on the size of the primary particles (*i.e.*, $\phi_g \approx 0.8$ and 0.5, respectively, for $R_p = 21$ nm and 37.5 nm). A power-law scaling of the dimensionless gelation time τ_g with ϕ has been observed with a slope of -1.6. This can be explained by the specific crossover gelation kinetics near the gelation point.

Acknowledgements

This work has been financially supported by the Suisse National Science Foundation (Grant no. 200020_126487/2). The MFA latexes supplied by Solvay Italy and fruitful discussion with Alessio Zaccone and Marco Lattuada are gratefully acknowledged.

References

1 F. Sciortino and P. Tartaglia, *Adv. Phys.*, 2005, **54**, 471–524.
2 E. Zaccarelli, *J. Phys.: Condens. Matter*, 2007, **19**, 323101.
3 V. Trappe and P. Sandkühler, *Curr. Opin. Colloid Interface Sci.*, 2004, **8**, 494.
4 M. Carpineti and M. Giglio, *Phys. Rev. Lett.*, 1992, **68**, 3327.
5 F. Sciortino and P. Tartaglia, *Phys. Rev. Lett.*, 1995, **74**, 282–285.
6 A. H. Krall and D. A. Weitz, *Phys. Rev. Lett.*, 1998, **80**, 778.
7 K. Kroy, M. E. Cates and W. C. K. Poon, *Phys. Rev. Lett.*, 2004, **92**, 148302.
8 M. Lattuada, H. Wu and M. Morbidelli, *Langmuir*, 2004, **20**, 4355–4362.
9 M. Carpineti and M. Giglio, *Phys. Rev. Lett.*, 1993, **70**, 3828.
10 M. Mellema, J. W. M. Heesakkers, J. H. J. van Opheusden and T. van Vliet, *Langmuir*, 2000, **16**, 6847–6854.
11 H. Wu and M. Morbidelli, *Langmuir*, 2001, **17**, 1030–1036.
12 H. Wu, J. Xie, M. Lattuada and M. Morbidelli, *Langmuir*, 2005, **21**, 3291–3295.
13 V. Trappe, V. Prasad, L. Cipelletti, P. N. Segre and D. A. Weitz, *Nature*, 2001, **411**, 772.
14 J. Bergenholtz, W. C. K. Poon and M. Fuchs, *Langmuir*, 2003, **19**, 4493–4503.
15 S. Buzzaccaro, R. Rusconi and R. Piazza, *Phys. Rev. Lett.*, 2007, **99**, 098301.
16 F. Cardinaux, T. Gibaud, A. Stradner and P. Schurtenberger, *Phys. Rev. Lett.*, 2007, **99**, 118301–118304.
17 P. J. Lu, E. Zaccarelli, F. Ciulla, A. B. Schofield, F. Sciortino and D. A. Weitz, *Nature*, 2008, **453**, 499–503.
18 W. C. K. Poon and M. D. Haw, *Adv. Colloid Interface Sci.*, 1997, **73**, 71–126.
19 P. N. Pusey and W. van Megen, *Phys. Rev. Lett.*, 1987, **59**, 2083.
20 W. van Megen and S. M. Underwood, *Phys. Rev. E: Stat. Phys., Plasmas, Fluids, Relat. Interdiscip. Top.*, 1994, **49**, 4206.
21 H. Wu, A. Zaccone, A. Tsoutsoura, M. Lattuada and M. Morbidelli, *Langmuir*, 2009, **25**, 4715–4723.
22 C. M. Sorensen and A. Chakrabarti, *Soft Matter*, 2011, **7**, 2284–2296.
23 P. Sandkühler, J. Sefcik and M. Morbidelli, *J. Phys. Chem. B*, 2004, **108**, 20105–20121.
24 H. Wu, J. Xie, M. Lattuada, J. Kohlbrecher and M. Morbidelli, *J. Phys. Chem. C*, 2011, **115**, 931–936.
25 M. Lattuada, H. Wu and M. Morbidelli, *Phys. Rev. E: Stat., Nonlinear, Soft Matter Phys.*, 2001, **64**, 061404.
26 M. Lattuada, H. Wu, A. Hasmy and M. Morbidelli, *Langmuir*, 2003, **19**, 6312–6316.
27 P. Sandkühler, J. Sefcik and M. Morbidelli, *Langmuir*, 2005, **21**, 2062–2077.
28 M. Lattuada, P. Sandkühler, H. Wu, J. Sefcik and M. Morbidelli, *Adv. Colloid Interface Sci.*, 2003, **103**, 33–56.
29 M. Lattuada, H. Wu, P. Sandkuhler, J. Sefcik and M. Morbidelli, *Chem. Eng. Sci.*, 2004, **59**, 1783.
30 P. Sandkühler, M. Lattuada, H. Wu, J. Sefcik and M. Morbidelli, *Adv. Colloid Interface Sci.*, 2005, **113**, 65–83.
31 M. Rottereau, J. C. Gimel, T. Nicolai and D. Durand, *Eur. Phys. J. E*, 2004, **15**, 133–140.
32 H. Wu, J. Xie and M. Morbidelli, *Biomacromolecules*, 2005, **6**, 3189–3197.
33 L. Ehrl, M. Soos and M. Lattuada, *J. Phys. Chem. B*, 2009, **113**, 10587–10599.